Magnetic properties of half metal studied by the DFT+DMFT approach in paramagnetic phase: the case of CrO_2

Andrey A. Katanin[1,2⋆]

1 Center for Photonics and 2D Materials, Moscow Institute of Physics and Technology, Institutsky lane 9, Dolgoprudny, 141700, Moscow Region, Russia
2 M. N. Mikheev Institute of Metal Physics of Ural Branch of Russian Academy of Sciences, S. Kovalevskaya Street 18, 620990 Yekaterinburg, Russia

⋆ Andrey.Katanin@gmail.com ,

Abstract

Magnetic properties of CrO_2 are studied within the density functional theory plus dynamical mean-field theory (DFT+DMFT) approach in the paramagnetic phase. While the magnon dispersion in the 3-orbital model, containing only t_{2g} states, possesses negative branches in accordance with previous studies in ferromagnetic phase, this drawback is removed in the 5-orbital model, including all d-states. The model including oxygen states (with purely local interaction at chromium sites) overestimates the exchange interactions and spin wave stiffness, pointing to important contributions of double exchange in CrO_2.

Received Date
Accepted Date
Published Date

1 Introduction

Half metals represent an important class of magnetic materials, see, e.g., the review [1]. Having gapped minority spin band at the Fermi level in the ferromagnetic state, these systems can possess large magnetic moment, which finds its industrial applications. The properties of these systems are expected to be somewhat different from the strong magnets with both, minority and majority states present at the Fermi level. In the latter case large magnetic moment originates from the electron localization induced by Hund exchange [2–4] and exchange interaction is of RKKY type [5–7].

The prominent example of half metals with large magnetic moment is CrO_2, which has Curie temperature $T_C \simeq 390$ K and saturation magnetic moment $\mu_s \simeq 2\mu_B$ per formula unit [8, 9]. The magnetic susceptibility shows the Curie-Weiss law with the square of magnetic moment $\mu^2_{\rm CW} = (8.3 \pm 0.3)\mu_B^2$ determined from the slope of inverse susceptibility [8, 10], which also corresponds to the effective spin $S_{\rm eff} \simeq 1$, in agreement with the above mentioned saturation magnetic moment. These features can be considered as an indication of strong magnetism with well formed local magnetic moments.

Near the Curie temperature, when the Stoner splitting is small, strong magnetic half metals are expected to reveal closer similarity to the other strong magnets. The important question is therefore whether magnetic properties of these systems originate from the presence of local magnetic moments, and whether they strongly change between the low-temperature limit and

in the proximity of Curie temperature. The related problem is whether the effects of interaction in such strong half metal magnets are more important than pecularities of band structure yielding half metallicity. Several experimental observations (photoemission, soft-x-ray absorption and resistivity) show importance of correlation effects in CrO_2 [11–14]. Moderate correlation effects were also observed in the angle-resolved photoemission (ARPES) experiments [15]. The conclusions of the latter study are also supported by bulk-sensitive photoemission data, reported in Ref. [15], unveiling the occupied band structure of CrO_2 in the magnetic phase.

On the theoretical side, the density functional theory (DFT) calculations of CrO_2 [9,16–18] revealed splitting of the d states into the low lying t_{2g} states, which cross the Fermi level, and hybridyzed with the oxygen states, and the e_g states, pushed above the Fermi level. In turn, the t_{2g} states are split into the lower xy state and $yz \pm xz$ excited states (the notation of the states refer to the local coordinate frame). The dispersion of the xy states is almost flat, which promotes the interaction effects. In particular, the localization of the xy states by the interaction effects was suggested in Ref. [19]. The importance of correlation effects was also emphasized in the subsequent L(S)DA+DMFT studies [15, 20–23].

In accordance with the localization of the xy t_{2g} states and more itinerant nature of the $yz+xz$ states the double exchange nature of magnetic exchange was proposed in Refs. [19,24]. Yet, recent experimental studies did not find mixed valence of chromium atoms [25, 26], in contrast to the previous results [27]. The exchange interactions in CrO_2 were studied using the DFT [28,29], Hartree-Fock [29–31], and the combination of DFT with the dynamical mean field theory (DFT+DMFT) approach [29], which produce diverse values of exchange interactions. Application of the DFT+DMFT approach to the effective 3-orbital model, containing t_{2g} states only, produced negative branches of the magnon dispersion, pointing to the instability of ferromagnetism in that model [29]. The authors of Ref. [29] suggested inclusion of the oxygen states to stabilize the ferromagnetism. Therefore, despite long history of studying CrO_2, there is no common view on the mechanism of magnetic exchange and the magnitude of exchange interactions in this material.

Recently, the DFT+DMFT approach to treat the exchange interactions in the paramagnetic state was proposed [32]. This approach provides a possibility to study exchange interactions without imposing certain magnetic order, which allows one to obtain an unbiased information about these interactions. For strong half metals, like CrO_2 this may also help to emphasize the effect of correlations, especially near Curie temperature, where the corresponding magnetic splitting of the states is small.

In the present paper we revisit the problem of magnetism of CrO_2 within the DFT+DMFT approach. We show that in agreement with the earlier considerations the xy t_{2g} states appear to be more localized. We furthermore apply the recently proposed technique of calculation of exchange interactions in paramagnetic phase within the DFT+DMFT approach [32]. Using the obtained exchange interactions, we also obtain magnon dispersions and show that they are qualitatively and semi-quantitatively similar to those obtained in the ferromagnetic state. Remarkably, the magnon dispersion in the 5-orbital model (per chromium site) is positively definite, providing stability of ferromagnetism due to the e_g states.

Therefore, on the basis of these results, we show that magnetic properties of half metals can be well described starting from the paramagnetic phase, showing the correspondence of the properties of the symmetric and symmetry broken phases of these systems. Among considered models, we find that the low enenrgy 5-orbital model (per Cr site), is quantitatively sufficient to describe ferromagnetism of CrO_2. We argue that 11-orbital model (per Cr site) requires considering effects of the non-local Coulomb interaction.

2 Methods

2.1 DFT

The CrO_2 has $P4_2/mnm$ space group (point symmetry group D_{4h}). The DFT calculations were performed using the pseudo-potential method implemented in the Quantum Espresso [33] package supplemented by the maximally localized Wannier projection onto $3d$ states of Cr performed within Wannier90 package [34], which produces the resulting tight-binding 5-orbital model (here and in the following we specify the number of the orbitals per Cr site, the actual number of orbitals in the respective models is doubled because of the two sites in the unit cell). For comparison, we also considered the tight-binding Hamiltonian, which includes the p oxygen states, resulting in the 11-orbital model per Cr site. We use the lattice parameters $a = 4.422$Å, $c = 2.916$Å [29, 35]. The reciprocal space integration was performed using $16 \times 16 \times 16$ **k**-point grid.

The resulting band structure and the density of states are shown in Fig. 1. The e_g (t_{2g}) states can be constructed in the 5-orbital model by choosing the symmetric (antisymmetric) combination of d_{xy} and $d_{3z^2-r^2}$ states, as well as d_{xz} and d_{yz} states in the global reference frame (we perform the transformation $d_{yz} \to -d_{yz}$ and $d_{xy} \to -d_{xy}$ on one of the two chromium sites); the third t_{2g} state is identified with the $d_{x^2-y^2}$ state in the global reference frame, see Ref. [29]. We choose the rotation angles between the above mentioned states to diagonalize the crystal field; the obtained angle θ_1 of mixing of d_{xy} and $d_{3z^2-r^2}$ states is close to $\pi/6$ and for another pair of states it is equal to $\pi/4$. We note that Wannier functions of the d states in the 5-orbital model contain also an admixture of the oxygen states near the Fermi level (see Appendix A), while in 11 orbital model the hybridization is accounted via the hopping parameters. To construct the model with 3 orbitals per Cr site, corresponding to considering only t_{2g} states, we project out the resulting e_g states in the 5-orbital model as $H_{\text{eff}} = H_{t_{2g}} + H_{t_{2g},e_g}[\mu_{\text{DFT}} - H_{e_g}]^{-1}H_{e_g,t_{2g}}$, where μ_{DFT} is the DFT chemical potential and H_i and H_{ij} ($i, j = e_g, t_{2g}$) are the respective diagonal and off-diagonal blocks of the tight-binding Hamiltonian. We have verified, that the resulting Hamiltonian reproduces correctly the dispersion of the t_{2g} states close to the Fermi level, see Fig. 1.

2.2 DMFT

In DMFT calculations we consider the density-density interaction matrix, see the details in Ref. [32]. For the 5-orbital and 11-orbital models we have parameterized the interaction at the Cr sites by Slater parameters $F^0 = 1.99$ eV, $F^2 = 7.67$ eV, and $F^4 = 5.48$ eV, as obtained in Ref. [31]. For the 3-orbital model we use the Kanamori parameterization with the interactions $U_K = 2.84$ eV and $J_K = 0.70$ eV, obtained in Refs. [29, 31]. The corresponding Slater parameters (see, e.g., Supplementary Material of Ref. [36]) $U_S = 1.91$ eV, $J_S = 1.17$ eV. The parameter U_S is smaller than the corresponding parameter $U_S = F^0$ of the 5-orbital model due to screening of the interaction. For 11-orbital model we use a double-counting correction $H_{\text{DC}} = M_{\text{DC}} \sum_{ir} n_{ird}$ in the around mean-field form [37],

$$M_{\text{DC}} = \langle n_{ird} \rangle [U_S(2n_{\text{orb}}-1) - J_S(n_{\text{orb}}-1)]/(2n_{\text{orb}}), \tag{1}$$

where n_{ird} is the operator of the number of d electrons at the site (i, r), i is the unit cell index and r is the site index within the unit cell, n_{orb} is the number of considered orbitals per site, $J_S = (F^2 + F^4)/14$. We have verified that the fully localized form of the double counting produces quite close results.

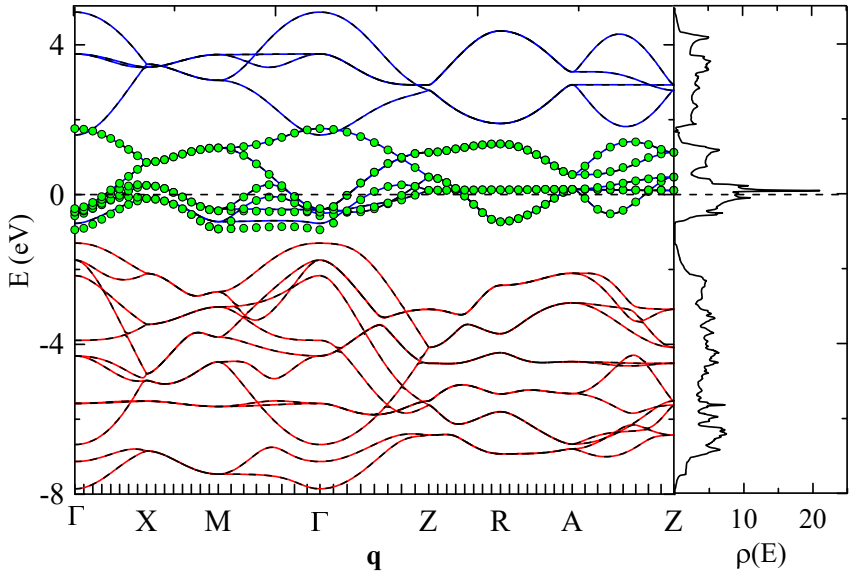

Figure 1: Left plot: band structure (dashed lines) and its wannierization (solid lines) in 5-orbital model (per Cr site, including only d states, blue lines) and 11-orbital (per Cr site, including d states of chromium and p states of oxygen, red and blue lines) models. The green circles show the band structure of the reduced t_{2g} states model (3 orbitals per Cr site, see text). Right plot shows the respective density of states.

2.3 Treatment of the d-p inetraction

Apart from the standard Coulomb repulsion in the chromium d-shell, parameterized by Slatter parameters, we consider also a model including the d-p chromium-oxygen interaction U_{dp}, as well as the repulsion between oxygen p-states, parameterized by Kanamori parameters U_{pp}, U'_{pp}, and J_{pp}, with the Hamiltonian

$$H_{dp} = U_{dp}\sum_{\langle ij\rangle} n_i n_j + U_{pp}\sum_{j,m} n_{jm\uparrow}n_{jm\downarrow} + \frac{U'_{pp}-J_{pp}}{2}\sum_{j,m\neq m',\sigma} n_{jm\sigma}n_{jm'\sigma} + \frac{U'_{pp}}{2}\sum_{j,m\neq m',\sigma} n_{jm\sigma}n_{jm',-\sigma}, \tag{2}$$

where i numerates chromium sites, j numerates oxygen sites, $\langle ij\rangle$ denotes nearest neighbours, $n_i = \sum_{m\sigma} n_{im\sigma}$, and $n_{im\sigma} = c^+_{im\sigma}c_{im\sigma}$. We treat these interactions within the static mean field approximation, assuming approximately equal occupations of oxygen p-orbitals, characterized by total occupation $\langle n_{\rm O}\rangle$ per oxygen atom,

$$H^{\rm MF}_{dp} = \left[U_{dp}z_O\langle n_{\rm Cr}\rangle + \widetilde{U}_{pp}\langle n_{\rm O}\rangle\right]\sum_j n_j + U_{dp}z_{\rm Cr}\langle n_{\rm O}\rangle\sum_i n_i, \tag{3}$$

where $\widetilde{U}_{pp} = U_{pp}/(2n_p) + (U'_{pp} - J_{pp}/2)(1-1/n_p)$, $n_p = 3$ is the number of p-orbitals, $z_{\rm Cr} = 6$, $z_{\rm O} = 3$ are the coordination (nearest neighbour) numbers of chromium and oxygen sites, $\langle n_{\rm Cr}\rangle$ is the respective chromium occupation of Cr per atom. Following Ref. [38], we substract the double counting contribution, which is equal to the oxygen and chromium energy shifts in Eq. (3) with the DFT occupations $\langle n_{\rm Cr}\rangle_0$ and $\langle n_{\rm O}\rangle_0$. The resulting energy shifts of the chromium and oxygen states are given by

$$\begin{aligned}\Delta E_{\rm Cr} &= U_{dp}z_{\rm Cr}\left[\langle n_{\rm O}\rangle - \langle n_{\rm O}\rangle_0\right] = -U_{dp}z_{\rm Cr}\left[\langle n_{\rm Cr}\rangle - \langle n_{\rm Cr}\rangle_0\right]/r, \\ \Delta E_{\rm O} &= U_{dp}z_{\rm O}\left[\langle n_{\rm Cr}\rangle - \langle n_{\rm Cr}\rangle_0\right] + \widetilde{U}_{pp}\left[\langle n_{\rm O}\rangle - \langle n_{\rm O}\rangle_0\right] = \left(U_{dp}z_{\rm O} - \widetilde{U}_{pp}/r\right)\left[\langle n_{\rm Cr}\rangle - \langle n_{\rm Cr}\rangle_0\right],\end{aligned} \tag{4}$$

where $r = 2$ is the ratio of oxygen and chromium sites in the formula unit, and we have taken into account that the total number of electrons $\langle n_{\rm Cr}\rangle + r\langle n_{\rm O}\rangle = \langle n_{\rm Cr}\rangle_0 + r\langle n_{\rm O}\rangle_0$ is conserved. Finally, absorbing the shift $\Delta E_{,\rm Cr}$ at the chromium sites into the chemical potential $\mu \to \mu + U_{dp} z_{\rm Cr}[\langle n_{\rm Cr}\rangle - \langle n_{\rm Cr}\rangle_0]/r$, we find the energy shift of oxygen p-states

$$\Delta E'_{\rm O} = (z_{\rm O} + z_{\rm Cr}/r)\widetilde{U}_{dp}[\langle n_{\rm Cr}\rangle - \langle n_{\rm Cr}\rangle_0] \tag{5}$$

where $\widetilde{U}_{dp} = U_{dp} - \widetilde{U}_{pp}/(rz_{\rm O} + z_{\rm Cr})$. In DMFT calculation we account for this energy shift as (taken with the opposite sign) double counting correction of the oxygen p-states. The parameter $\widetilde{U}_{dp}$ controls the energy shift of oxygen states. For calculations we consider the parameters $U_{pp} = 1.5$eV, $J_{pp} = 0.5$eV, $U_{dp} = 0.65$eV, $U'_{pp} = U_{pp} - 2J_{pp}$, which yield $\widetilde{U}_{dp} \simeq 0.6$eV. Since the screening of d-d interaction by p states is beyond the Hartree-Fock approximation, we use the same parameters of the local interaction within d-shell, as for the 5-orbital model.

2.4 Exchange interactions

To determine the exchange interactions we consider the effective Heisenberg model with the Hamiltonian $H = -(1/2)\sum_{\mathbf{q},rr'} J^{rr'}_{\mathbf{q}} \mathbf{S}^{r}_{\mathbf{q}} \mathbf{S}^{r'}_{-\mathbf{q}}$, $\mathbf{S}^{r}_{\mathbf{q}}$ is the Fourier transform of static operators $\mathbf{S}_{ir}$, where the orbital-summed on-site static spin operators $\mathbf{S}_{ir} = \sum_m \mathbf{S}_{irm}$ and

$$\mathbf{S}_{irm} = \frac{1}{2}\sum_{\sigma\sigma'\nu} c^{+}_{irm\sigma\nu} \boldsymbol{\sigma}_{\sigma\sigma'} c_{irm\sigma'\nu} \tag{6}$$

is the electron spin operator, ν are the Matsubara frequencies, $c^{+}_{irm\sigma\nu}$ and $c_{irm\sigma\nu}$ are the frequency components of the electron creation and destruction operators at the site (i,r), d-orbital m, and spin projection σ, and $\boldsymbol{\sigma}_{\sigma\sigma'}$ are the Pauli matrices.

We relate exchange parameters $J_{\mathbf{q}}$ to the orbital-summed non-local static longitudinal susceptibility $\chi^{rr'}_{\mathbf{q}} = -\langle\langle S^{z,r}_{\mathbf{q}} | S^{z,r'}_{-\mathbf{q}}\rangle\rangle_{\omega=0} = \sum_{mm'} \hat{\chi}^{mr,m'r'}_{\mathbf{q}}$ (the hats stand for matrices with respect to orbital and site indexes; $\langle\langle ..|..\rangle\rangle_\omega$ is the retarded Green's function), by (see Refs. [32,39,40]) $J_{\mathbf{q}} = \chi^{-1}_{\rm loc} - \chi^{-1}_{\mathbf{q}}$, the matrix inverse is taken with respect to the site indexes in the unit cell. The matrix of local susceptibilities $\chi^{rr'}_{\rm loc} = -\langle\langle S^{z}_{ir} | S^{z}_{ir}\rangle\rangle_{\omega=0}\delta_{rr'} = \sum_{mm'} \hat{\chi}^{mm',r}_{\rm loc}\delta_{rr'}$ is diagonal with respect to the site indexes. The non-local susceptibility is determined from the Bethe-Salpeter equation using the local particle-hole irreducible vertices [41], accounting also the corrections for the finite frequency box (cf. Refs. [32, 42]). The local irreducible vertices are extracted from the inverse Bethe-Salpeter equation applied to the local particle-hole vertex obtained within the DMFT [41].

The DMFT calculations of the self-energies, non-uniform susceptibilities and exchange interactions were performed using the continous time Quantum Monte Carlo method of the solution of impurity problem [43], realized in the iQIST software [44], see also Refs. [32,39].

3 Results

In Fig. 2(a) we show the partial densities of states for $\beta = 10$ eV^{-1}, compared to those in DFT approach. The occupation of Cr sites is fixed to 2 electrons per site in 3- and 5-orbital models, corresponding to fixed valence of Cr sites. The respective hybridized low energy oxygen and chromium states, forming Wannier functions, are considered as interacting ones. At the same time, in 11-orbital model the occupation is determined by the total filling of 28 electrons per unit cell, and constitutes 3.75 per Cr site (see fillings of the d orbitals in Table 1 and density-density correlators in Appendix B). The increase of the filling originates from strong

	$n(l_{xy})$	$n(l_{xz-yz})$	$n(l_{xz+yz})$	$n(l_{3z^2-r^2})$	$n(l_{x^2-y^2})$	n_d
3-orb	0.49	0.34	0.17	0	0	2
5-orb	0.47	0.36	0.14	0.02	0.01	2
11-orb	0.52	0.45	0.39	0.27	0.26	3.75
11-orb + $U_{dp,pp}$	0.48	0.40	0.25	0.16	0.15	2.87

Table 1: Fillings $n(l)$ of d-orbitals l_α per one spin projection and the total filling of d-states n_d in DFT+DMFT approach. The notation of the orbitals refer to the local coordinate frame; the fillings are estimated at $\beta = 10$ eV^{-1}, but only weakly depend on temperature.

hybridization of chromium and oxygen states, as discussed earlier in DFT approaches [9, 16–19, 24].

In Figs. 2(b,c) we show the frequency depndence of the electronic self-energies. In agreement with previous considerations, the two of the three t_{2g} states $l_{xy} = \cos\theta_1 d_{3z^2-r^2} - \sin\theta_1 d_{xy}$ and $l_{xz-yz} = (d_{xz} - d_{yz})/\sqrt{2}$ (the indexes of l_i refer to the local reference frame according to Refs. [18, 19, 29]) appear to have larger damping, and, respectively, more localized. On the other hand, the t_{2g} state $l_{xz+yz} = d_{x^2-y^2}$, as well as e_g states have smaller damping, and appear to be more itinerant. Closer proximity of the t_{2g} states l_{xy} and l_{xz-yz} to half filling in the 11-orbital model provides enhancement of correlations (cf. Ref. [45]), in particular non-quasiparticle form of the self-energy of these states with $\partial \mathrm{Im}\Sigma(i\nu)/\partial\nu = \partial \mathrm{Re}\Sigma(\nu)/\partial\nu > 0$ at small frequencies, which yields larger local magnetic moments (see below).

To treat properly hybridization of d and p states, we additionally consider the 11-orbital model, including repulsion U_{pp} between oxygen p states, as well as non-local interaction U_{dp} between chromium d and oxygen p states within the static mean-field approximation, together with DMFT for the chromium d states (see Sect. 2.3). The respective fillings (see Table 1) in the presence of these additional interactions become closer to the 5-orbital model; the filling of chromium d states constitutes in this case 2.87 electrons. The results for the spectral function and self-energy of the 11-orbital model with included interactions U_{pp} and U_{dp} are shown in Fig. 3. One can see that the shift of p-states leads to suppression of $d-p$ hybridization, such that both, the spectral functions and self-energy become close to those in 5-orbital model.

One can also see that, in agreement with the earlier studies [23], in all considered models the peak of the density of states, which is present in DFT approach at the Fermi level, is pushed to the energy $\nu_{\mathrm{peak}} \sim -0.5$ eV in DFT+DMFT approach. We have verified that the l_{xy} state in the considered 5- and 11-orbital models provides largest contribution to the peak of the density of states close to the Fermi energy, which shift can be therefore identified with the large quasiparticle damping of the corresponding states. This shift is therefore similar to the earlier discussed in two-dimensional systems gap formation in the vicinity of the antiferromagnetic state [46] and the Fermi surface quasi-splitting near the ferromagnetic instability [47, 48], although in the present case large damping occurs due to electronic, rather than magnetic correlations, which implies (similarly to the antiferromagnetic state) that it does not depend on the momentum (being almost local in real space).

The temperature dependence of the inverse uniform $\chi_{\mathbf{q}=0} = \chi^{11}_{\mathbf{q}=0} + \chi^{12}_{\mathbf{q}=0}$ and local

$$\chi_{\mathrm{loc}} = -\langle\langle S^z_{ir} | S^z_{ir} \rangle\rangle_{\omega=0} = \sum_{mm'} \hat{\chi}^{mm',r}_{\mathrm{loc}} \tag{7}$$

susceptibilities in the 3- and 5-orbital models, as well as 11-orbital models, is almost linear, as shown in Fig. 4, which points to the existence of well formed local magnetic moments. The Curie temperatures, obtained from vanishing of inverse uniform susceptibility are presented

in Table 2. Due to the mean-field nature the dynamical men-field theory approach is known to overestimate Curie temperature. Therefore, obtained Curie temperatures can be considered as an upper bound and corrected below with account of the non-local correlations.

From the slope of inverse local and uniform magnetic susceptibilities we extract the local magnetic moments $\mu^2_{\rm loc}$ and μ^2 according to

$$\chi^{-1}_{\rm loc} = 3(g\mu_B)^2(T+T_W)/\mu^2_{\rm loc}, \tag{8}$$
$$\chi^{-1}_{\mathbf{q}=0} = 3(g\mu_B)^2(T-T_C)/\mu^2 \tag{9}$$

where $g = 2$ (see Table 2). In terms of the effective spin, defined by $g^2 S_{\rm eff}(S_{\rm eff}+1) = \mu^2_{\rm loc}$, this corresponds to $S_{\rm eff} = 1.2$ for three- and five-orbital models and $S_{\rm eff} = 1.27$ for the 11-orbital models. We note that the magnetic moments, especially extracted from local magnetic susceptibility, are somewhat overestimated in the considered density-density approximation, which neglects transverse components of Hund exchange, see Refs. [36, 49]. From the uniform susceptibility we obtain somewhat smaller magnetic moments, which are in a reasonable agreement with the experimental data ($\mu^2/\mu_B^2 = 8.3 \pm 0.3$, Refs. [8, 10]). The Weiss temperature T_W of the inverse local magnetic susceptibility appears to be quite small, showing smallness of the Kondo temperature [50, 51].

	$(\mu_{\rm loc}/\mu_{\rm B})^2$	$(\mu/\mu_{\rm B})^2$	$T_C^{\rm DMFT}$	$T_C^{\rm fluct}$
3-orb	10.6	8.0	897	-
5-orb	10.4	7.8	1350	540
11-orb	11.7	8.9	1700	850
11-orb + $U_{dp,pp}$	11.4	8.7	1470	820
Experimental		8.3±0.3		390

Table 2: Magnetic moments and Curie temperatures in DFT+DMFT approach. The notation of the orbitals refer to the local coordinate frame.

Using the approach of Refs. [32, 39, 40] we obtain the exchange interactions $J^{rr'}_{\mathbf{q}}$. We note that having smaller bandwidth, and fully filled oxygen p states well below the Fermi level, the 5-orbital model describes magnetic exchange mechanism similar to the double exchange type. At the same time, uncorerrelated oxygen states in 11-orbital model mediate magnetic exchange of RKKY type. The Fourier transformation of the obtained exchange interactions at $\beta = 10$ eV^{-1} is presented in Table 3. The obtained exchange interactions are comparable to those obtained in the ferromagnetic state in Refs. [29, 31], with the exchange interactions between the nearest neighbour sites larger in the presence of the oxygen states, than in the 3- and 5-orbital models, due to larger hybridization of chromium states. With including U_{dp} and U_{pp}

$N_{\rm orb}$	J_1	J_2	J_3	J_4	J_5	J_6	$J_7^>$	$J_7^<$	$J_8^>$	$J_8^<$
3	11.4	0.1	0.6	0.1	−0.5	−2.1	−5.6	−2.0	−2.0	−2.0
5	14.8	17.8	0.6	0.2	−0.5	−1.7	−5.2	−1.2	−1.9	−1.1
11	25.5	18.1	1.8	0.6	−1.1	−2.0	−5.0	−2.0	−2.0	−1.4
11-orb+$U_{dp,pp}$	8.8	18.0	−0.1	0.1	−0.4	−0.6	−2.9	−0.7	−0.7	−1.1

Table 3: Exchange interactions (in meV) between various chromium sites at $\beta = 10$ eV^{-1} for the 3- and 5 orbital models per chromium site, as well as 11-orbital models, including oxygen states. $11dp$ stands for the model with U_{dp}, U_{pp} interactions. The notation of the exchange interactions is the same as in Refs. [29, 31].

interactions, the nearest neighbour exchange is suppressed in 11-orbital model; the antiferromagnetic exchanges at longer distances are however also suppressed, reducing frustration effects.

Using the obtained exchange interactions in the temperature range $T \gtrsim T_C$, we obtain magnon dispersion as the $\mathbf{q}$-dependent eigenvalues of the matrix of the spin-wave Hamiltonian (cf. Refs. [39, 40]), assuming that the exchange interactions do not change strongly with lowering the temperature. The resulting magnon dispersions are shown in Fig. 5. One can see that the magnon dispersion of the 3-orbital model possesses negative branches, showing an instability of ferromagnetism, similarly to previous study in the ferromagnetic phase [29]. At the same time, the magnon dispersions of the 5-orbital model are positive definite, providing the stability of the ferromagnetic state. Therefore, inclusion of the e_g states seems to be crucial for the stability of ferromagnetism. The maximal energy of the obtained magnon dispersion in the 5-orbital model is larger than that in the "method $\hat{b}$" of Ref. [31], corresponding to the infinitesimal rotation of exchange-correlation potential, but comparable to that obtained in the "method $\hat{m}$" of Ref. [31] (considering infinitesimal rotation of magnetization). The dispersion in the model including oxygen states without additional U_{dp} and U_{pp} interactions is somewhat larger than in the 5-orbital model due to larger exchange interactions, but becomes comparable to that for the 5-orbital model with account of $U_{dp,pp}$ interactions.

The temperature dependencies of the obtained spin-wave stiffnesses in the 5-orbital model in various directions are shown in Fig. 6. One can see that the average spin-wave stiffness, extrapolated to the low-temperature limit, $D_{\text{av}} \simeq 110$ meV·Å^2 is in a reasonable agreement with the experimental data $D = 60$ to 150 meV·Å^2, Refs. [52–54]. At the same time, the 11-orbital models yield larger value of the spin-wave stiffness, $D_{\text{av}} \gtrsim 200$ meV·Å^2 (not shown). Although the interactions $U_{dp,pp}$ yield the suppression of exchange interactions and the spin wave stiffness D_z in 11-orbital model, spin wave stiffness D_{xy} is increased by these interactions due to suppression of antiferromagnetic exchange interactions $J_{7,8}$ (the suppressed ferromagnetic interaction J_1 acts along the z axis and therefore contributes to D_z only). This may show, that for accurate description of the low-energy magnon dispersion in 11-orbital model the treatment of the non-local interaction beyond simplest static mean field approximation is required.

Finally, to estimate the non-local corrections to the Curie temperature beyond DMFT, we use the RPA approach [55], see also Ref. [39]. Assuming that the sites of the unit cell are equivalent, we find

$$T_C = \frac{\mu^2}{3(g\mu_B)^2 \sum_{\mathbf{q}} \left[\lambda \delta_{rr'} - J^{rr'}_{\mathbf{q}}\right]^{-1}_{11}}, \tag{10}$$

where $\lambda = \sum_{r'} J^{rr'}_0$. The obtained results taking the obtained exchange interactions at $\beta = 10\,\text{eV}^{-1}$ are presented in Table 2. With account of the non-local corrections, the Curie temperature is suppressed with respect to the DMFT Curie temperature, and for the 5-orbital model only moderately overestimates experimental data. For the 11-orbital models the Curie temperature is stronger overestimated; for the model including $U_{dp,pp}$ interactions the suppression of Curie temperature with respect to DMFT appears not too strong because of weakened frustration effects in this model.

The success of the 5-orbital model in description of the magnetic properties of CrO_2 relies on the fact that this model is better suited to describe double exchange interaction, having also lower band width, comparable to Hund exchange interaction. Describing the double exchange interaction within 11-orbital model requires accurate (possibly, non-perturbative) treatment of the non-local Coulomb interactions.

4 Conclusion

In summary, we have evaluated non-uniform susceptibilities, Curie temperatures, and exchange interactions in 3-, 5-, and 11-orbital (per Cr site) models within DFT+DMFT approach. The most reasonable results are obtained within the low-energy 5-orbital model, representing double exchange interaction. This model yields positive magnon dispersions and reasonable Curie temperature, although the latter is still overestimated with respect to the experimental data. The overestimate of the Curie temperature is likely connected with the assumed density-density form of the Coulomb interaction (cf. Ref. [36]), presence of magnetic frustrations, etc. We show also that the considered approach allows for a correct description of the experimental data for the spin-wave stiffness.

At the same time, the 11-orbital model, including oxygen states, yields strong hybridization of these states with chromium states at the energies well below the Fermi level, which results in the filling of d-orbitals of Cr closer to half filling, and therefore stronger correlations. Remarkably, we find RKKY mechanism of magnetic exchange, represented by 11-orbital model with local Coulomb interaction, inapplicable even in paramagnetic phase of CrO_2. We argue that considering non-local interaction between chromium and oxygen sites (together with U_{pp} interaction) within static mean field approximation increases occupation of oxygen p states and substantially improves the results for the 11-orbital model. At the same time, it yields larger spin-wave stiffness, than that for 5-orbital model and experimental data. Likely, treatment of non-local interactions beyond static mean-field approximation, e.g. within cluster methods or non-local extensions of dynamical mean-field theory [41, 42, 56–58], will further improve the results of this model.

The possibility of describing reasonably well magnetic properties of CrO_2 from the paramagnetic phase implies presence of the correspondence between the magnetic properties in ferro- and paramagnetic phases. Mathematically, this correspondence occurs due to compensation of the self-energy and vertex corrections to the spin susceptibility, which was discussed earlier in the ferro- [59] and paramagnetic [32] phases. The performed study also implies formation of local magnetic moments in CrO_2 due to Hund exchange interaction, and their double exchange-like interaction even in paramagnetic phase.

Further experimental and theoretical studies of the form of magnon dispersion, and its evolution from the low- to the high-temperature limit are of certain interest. Also describing the effect of the non-local chromium-oxygen interaction, as well as the consideration of magnetic properties of CrO_2 with full SU(2) symmetric Coulomb interaction has to be performed in future.

Acknowledgements

The author appreciates stimulating discussions with I. V. Solovyev at the early stage of the work. The calculations were performed on the cluster of the Laboratory of Material Computer Design of MIPT and the Uran supercomputer at the IMM UB RAS.

The DMFT calculations are supported by the project of Russian Science Foundation 24-12-00186. The DFT calculations are performed within the theme “Quant" 122021000038-7. of the Ministry of Science and Higher Education of the Russian Federation.

A Wannier orbitals in 5- and 11-orbital models

In Figs. 7 and 8 we visualize [60] Wannier orbitals in 5- and 11-orbital models (before performing basis rotation which diagonalises crystal field). One can see that in the 5-orbital model Wannier functions contain substantial admixture of the oxygen states, originating from the bands the vicinity of the Fermi level, while in 11-orbital model Wannier functions are more localized at chromium and oxygen sites. As it is discussed in the main text in the latter model however the hybridization occurs via the hopping parameters, which in particular yield additional contribution to the density of d states at the energies well below the Fermi level ($\nu \sim -4$ eV).

B Density correlations in DFT+DMFT approach

In Tables 4, 5, and 6 we present the density-density correlation function $\langle n_{m\sigma} n_{m'\sigma'} \rangle$ in 5- and 11-orbital models in DFT+DMFT approach at $\beta = 10$ eV^{-1}. In the 5-orbital model the density correlation matrix has only few off-diagonal elements, the major one is between l_{xy} and l_{xz-yz} orbitals in the local coordinate frame, which have largest quasiparticle damping (see Fig. 2 of the main text). The 11-orbital model with local interaction possesses stronger off-diagonal correlations, which reflects stronger mixing of various orbiatl states in this model. On the other hand, in 11-orbital model with U_{dp} and U_{pp} interactions the correlations become more diagonal, and resemble the results for the 5-orbital model.

	$n_{1\uparrow}$	$n_{2\uparrow}$	$n_{3\uparrow}$	$n_{4\uparrow}$	$n_{5\uparrow}$	$n_{1\downarrow}$	$n_{2\downarrow}$	$n_{3\downarrow}$	$n_{4\downarrow}$	$n_{5\downarrow}$
$n_{1\uparrow}$	**0.47**	0.01	0.00	0.33	0.11	0.00	0.01	0.00	0.01	0.01
$n_{2\uparrow}$	0.01	**0.02**	0.00	0.01	0.00	0.01	0.00	0.00	0.00	0.00
$n_{3\uparrow}$	0.00	0.00	**0.01**	0.00	0.00	0.00	0.00	0.00	0.00	0.00
$n_{4\uparrow}$	0.33	0.01	0.00	**0.36**	0.07	0.01	0.00	0.00	0.00	0.01
$n_{5\uparrow}$	0.11	0.00	0.00	0.07	**0.14**	0.01	0.00	0.00	0.01	0.00
$n_{1\downarrow}$	0.00	0.01	0.00	0.01	0.01	**0.47**	0.01	0.00	0.33	0.11
$n_{2\downarrow}$	0.01	0.00	0.00	0.00	0.00	0.01	**0.02**	0.00	0.01	0.00
$n_{3\downarrow}$	0.00	0.00	0.00	0.00	0.00	0.00	0.00	**0.01**	0.00	0.00
$n_{4\downarrow}$	0.01	0.00	0.00	0.00	0.01	0.33	0.01	0.00	**0.36**	0.07
$n_{5\downarrow}$	0.01	0.00	0.00	0.01	0.00	0.11	0.00	0.00	0.07	**0.14**

Table 4: Density correlators $\langle n_{m\sigma} n_{m'\sigma'} \rangle$ in the 5-orbital model in DFT+DMFT approach at $\beta = 10$ eV^{-1}. The diagonal elements correspond to the respective fillings. The notation of the orbiatls: 1: l_{xy}, 2: $l_{3z^2-r^2}$, 3: $l_{x^2-y^2}$, 4: l_{xz-yz}, 5: l_{xz+yz}

References

[1] M. I. Katsnelson, V. Yu. Irkhin, L. Chioncel, A. I. Lichtenstein, and R. A. de Groot, *Half-metallic ferromagnets: From band structure to many-body effects*, Rev. Mod. Phys. **80**, 315 (2008), doi: https://doi.org/10.1103/RevModPhys.80.315.

[2] P. Werner, E. Gull, M. Troyer, and A. J. Millis, *Spin Freezing Transition and Non-Fermi-Liquid Self-Energy in a Three-Orbital Model*, Phys. Rev. Lett. **101**, 166405 (2008), doi: https://doi.org/10.1103/PhysRevLett.101.166405.

	$n_{1\uparrow}$	$n_{2\uparrow}$	$n_{3\uparrow}$	$n_{4\uparrow}$	$n_{5\uparrow}$	$n_{1\downarrow}$	$n_{2\downarrow}$	$n_{3\downarrow}$	$n_{4\downarrow}$	$n_{5\downarrow}$
$n_{1\uparrow}$	**0.52**	0.16	0.14	0.35	0.28	0.08	0.12	0.12	0.11	0.12
$n_{2\uparrow}$	0.16	**0.27**	0.07	0.12	0.11	0.12	0.06	0.06	0.10	0.09
$n_{3\uparrow}$	0.14	0.07	**0.26**	0.12	0.10	0.12	0.06	0.05	0.10	0.09
$n_{4\uparrow}$	0.35	0.13	0.12	**0.45**	0.23	0.11	0.10	0.10	0.09	0.11
$n_{5\uparrow}$	0.28	0.11	0.10	0.23	**0.39**	0.12	0.09	0.09	0.11	0.08
$n_{1\downarrow}$	0.08	0.12	0.12	0.11	0.12	**0.52**	0.15	0.14	0.35	0.28
$n_{2\downarrow}$	0.12	0.06	0.06	0.10	0.09	0.15	**0.27**	0.07	0.13	0.11
$n_{3\downarrow}$	0.12	0.06	0.05	0.10	0.09	0.14	0.07	**0.26**	0.12	0.10
$n_{4\downarrow}$	0.11	0.10	0.10	0.09	0.11	0.35	0.13	0.12	**0.45**	0.23
$n_{5\downarrow}$	0.12	0.09	0.09	0.11	0.08	0.28	0.11	0.10	0.23	**0.39**

Table 5: Density correlators in the 11-orbital model with local interaction in DFT+DMFT approach at $\beta = 10$ eV^{-1}. The notation of the orbiatls is the same as in the Table 4.

	$n_{1\uparrow}$	$n_{2\uparrow}$	$n_{3\uparrow}$	$n_{4\uparrow}$	$n_{5\uparrow}$	$n_{1\downarrow}$	$n_{2\downarrow}$	$n_{3\downarrow}$	$n_{4\downarrow}$	$n_{5\downarrow}$
$n_{1\uparrow}$	**0.48**	0.09	0.07	0.33	0.18	0.04	0.07	0.06	0.05	0.05
$n_{2\uparrow}$	0.09	**0.16**	0.02	0.07	0.04	0.07	0.02	0.02	0.05	0.03
$n_{3\uparrow}$	0.07	0.02	**0.15**	0.06	0.04	0.06	0.02	0.02	0.05	0.03
$n_{4\uparrow}$	0.33	0.07	0.06	**0.40**	0.14	0.05	0.05	0.05	0.04	0.04
$n_{5\uparrow}$	0.18	0.04	0.04	0.14	**0.25**	0.05	0.03	0.03	0.04	0.02
$n_{1\downarrow}$	0.04	0.07	0.06	0.05	0.05	**0.48**	0.09	0.08	0.33	0.18
$n_{2\downarrow}$	0.07	0.02	0.02	0.05	0.03	0.09	**0.16**	0.02	0.07	0.04
$n_{3\downarrow}$	0.06	0.02	0.02	0.05	0.03	0.08	0.02	**0.15**	0.06	0.03
$n_{4\downarrow}$	0.05	0.05	0.05	0.04	0.04	0.33	0.07	0.06	**0.40**	0.14
$n_{5\downarrow}$	0.05	0.03	0.03	0.04	0.02	0.18	0.04	0.03	0.14	**0.25**

Table 6: Density correlators in the 11-orbital model in DFT+DMFT approach with U_{dp} and U_{pp} interactions at $\beta = 10$ eV^{-1}. The notation of the orbiatls is the same as in the Table 4.

[3] A. A. Katanin, A. I. Poteryaev, A. V. Efremov, A. O. Shorikov, S. L. Skornyakov, M. A. Korotin, and V. I. Anisimov, *Orbital-selective formation of local moments in α-iron: First-principles route to an effective model*, Phys. Rev. B **81**, 045117 (2010), https://doi.org/10.1103/PhysRevB.81.045117.

[4] I. Leonov, A. I. Poteryaev, V. I. Anisimov, and D. Vollhardt, *Electronic Correlations at the α-γ Structural Phase Transition in Paramagnetic Iron*, Phys. Rev. Lett. **106**, 106405 (2011), https://doi.org/10.1103/PhysRevB.85.020401; Phys. Rev. B **85**, 020401(R) (2012); I. Leonov, A. I. Poteryaev, Yu. N. Gornostyrev, A. I. Lichtenstein, M. I. Katsnelson, V. I. Anisimov, and D. Vollhardt, *Electronic correlations determine the phase stability of iron up to the melting temperature*, Scientific Reports **4**, 5585 (2015), doi: https://doi.org/10.1038/srep05585.

[5] S. V. Vonsovsky, *Magnetism* (Wiley, New York, 1974).

[6] M. B. Stearns, *Why is iron magnetic?*, Physics Today **31**(4), 34 (1978), https://doi.org/10.1063/1.2994993.

[7] A. S. Belozerov, A. A. Katanin, and V. I. Anisimov, *Momentum-dependent susceptibilities and magnetic exchange in bcc iron from supercell DMFT calculations*, Phys. Rev. B **96**, 075108 (2017), https://doi.org/10.1103/PhysRevB.96.075108.

[8] B. L. Chamberland, Crit. Reviews in Solid State and Mater. Sciences, *The chemical and physical properties of CrO_2 and tetravalent chromium oxide derivatives*, **7**, 1 (1977), doi: http://dx.doi.org/10.1080/10408437708243431.

[9] K. Schwarz, *CrO_2 predicted as a half-metallic ferromagnet*, J. Phys. F: Met. Phys. **16**, L211 (1986), http://dx.doi.org/10.1088/0305-4608/16/9/002.

[10] F. J. Darnell and W. H. Cloud, Magnetic properties of chromium dioxide, Bull. Soc. Chim. France, 1164 (1965).

[11] T. Tsujioka, T. Mizokawa, J. Okamoto, A. Fujimori, M. Nohara, H. Takagi, K. Yamaura, and M. Takano, *Hubbard splitting and electron correlation in the ferromagnetic metal CrO_2*, Phys. Rev. B **56**, R15509 (1997), doi: https://doi.org/10.1103/PhysRevB.56.R15509.

[12] S. P. Lewis, P. B. Allen, and T. Sasaki, *Band structure and transport properties of CrO_2*, Phys. Rev. B **55**, 10253 (1997), https://doi.org/10.1103/PhysRevB.55.10253.

[13] C. B. Stagarescu, X. Su, D. E. Eastman, K. N. Altmann, F. J. Himpsel, and A. Gupta, *Orbital character of O-2p unoccupied states near the Fermi level in CrO_2*, Phys. Rev. B **61**, R9233(R) (2000), https://doi.org/10.1103/PhysRevB.61.R9233.

[14] D. J. Huang, L. H. Tjeng, J. Chen, C. F. Chang, W. P. Wu, S. C. Chung, A. Tanaka, G. Y. Guo, H.-J. Lin, S. G. Shyu, C. C. Wu, and C. T. Chen, *Anomalous spin polarization and dualistic electronic nature of CrO_2*, Phys. Rev. B **67**, 214419 (2003), https://doi.org/10.1103/PhysRevB.67.214419.

[15] F. Bisti, V. A. Rogalev, M. Karolak, S. Paul, A. Gupta, T. Schmitt, G. Güntherodt, V. Eyert, G. Sangiovanni, G. Profeta, and V. N. Strocov, *Weakly-Correlated Nature of Ferromagnetism in Nonsymmorphic CrO_2 Revealed by Bulk-Sensitive Soft-X-Ray ARPES*, Phys. Rev. X **7**, 041067 (2017), doi: https://doi.org/10.1103/PhysRevX.7.041067.

[16] S. Matar, G. Demazeau, J. Sticht, V. Eyert, and J. Kübler, *Etude de la structure électronique et magnétique de CrO_2*, J. Phys. I **2**, 315 (1992), https://doi.org/10.1051/jp1:1992145.

[17] S. P. Lewis, P. B. Allen, and T. Sasaki, *Band structure and transport properties of CrO_2*, Phys. Rev. B **55**, 10253 (1997), https://doi.org/10.1103/PhysRevB.55.10253.

[18] A. Yamasaki, L. Chioncel, A. I. Lichtenstein, and O. K. Andersen, *Model Hamiltonian parameters for half-metallic ferromagnets NiMnSb and CrO_2*, Phys. Rev. B **74**, 024419 (2006), doi: https://doi.org/10.1103/PhysRevB.74.024419.

[19] M. A. Korotin, V. I. Anisimov, D. I. Khomskii, and G. A. Sawatzky, *CrO_2: A Self-Doped Double Exchange Ferromagnet*, Phys. Rev. Lett. **80**, 4305 (1998), doi: https://doi.org/10.1103/PhysRevLett.80.4305.

[20] M. S. Laad, L. Craco, and E. Müller-Hartmann, *Orbital correlations in the ferromagnetic half-metal CrO_2*, Phys. Rev. B **64**, 214421 (2001), doi: https://doi.org/10.1103/PhysRevB.64.214421.

[21] L. Craco, M. S. Laad, and E. Müller-Hartmann, *Orbital Kondo Effect in CrO_2: A Combined Local-Spin-Density-Approximation Dynamical-Mean-Field-Theory Study*, Phys. Rev. Lett. **90**, 237203 (2003), doi: https://doi.org/10.1103/PhysRevLett.90.237203.

[22] L. Chioncel, H. Allmaier, E. Arrigoni, A. Yamasaki, M. Daghofer, M. I. Katsnelson, and A. I. Lichtenstein, *Half-metallic ferromagnetism and spin polarization in CrO_2* Phys. Rev. B **75**, 140406(R) (2007), doi: https://doi.org/10.1103/PhysRevB.75.140406.

[23] Mu-Yong Choi, *Hund's metallicity and orbital-selective Mott localization of CrO2 in the paramagnetic state*, ArXiv:1611.05568 doi: https://doi.org/10.48550/arXiv.1611.05568.

[24] P. Schlottmann, *Double-exchange mechanism for CrO_2*, Phys. Rev. B **67**, 174419 (2003), doi: https://doi.org/10.1103/PhysRevB.67.174419.

[25] Y. V. Piskunov, A. F. Sadykov, V. V. Ogloblichev, A. G. Smolnikov, A. P. Gerashenko, and P. Z. Si, *Valence state of chromium ions in the half-metallic ferromagnet CrO_2 probed by ^{53}Cr NMR* Phys. Rev. B **106**, 094428 (2022), doi: https://doi.org/10.1103/PhysRevB.106.094428.

[26] V. Chlan, A. A. Shmyreva, and H. Štěpánková, *Electronic structure of CrO_2 probed by NMR and DFT*, ArXiv:2311.12846, doi: https://doi.org/10.48550/arXiv.2311.12846.

[27] S. Seong, E. Lee, H. Woo Kim, B.I. Min, S. Lee, J. Dho, Y. Kim, J.-Y. Kim, J.-S. Kang, *Experimental evidence for mixed-valent Cr ions in half-metallic CrO_2: Temperature-dependent XMCD study*, Journ. Magn. Magn. Mater. **452**, 447 (2018), doi: https://doi.org/10.1016/j.jmmm.2017.12.080.

[28] H. Sims, S. J. Oset, W. H. Butler, J. M. MacLaren, M. Marsman, *Determining the anisotropic exchange coupling of CrO_2 via first-principles density functional theory calculations*, Phys. Rev. B **81**, 224436 (2010), doi: https://doi.org/10.1103/PhysRevB.81.224436.

[29] I. V. Solovyev, I. V. Kashin, and V. V. Mazurenko, *Mechanisms and origins of half-metallic ferromagnetism in CrO_2*, Phys. Rev. B **92**, 144407 (2015), doi: https://doi.org/10.1103/PhysRevB.92.144407.

[30] I. V. Solovyev, I. V. Kashin, V. V. Mazurenko, *Band filling dependence of the Curie temperature in CrO_2*, J. Phys.: Condens. Matter **28**, 216001 (2016), doi: https://doi.org/10.1088/0953-8984/28/21/216001.

[31] I. V. Solovyev, *Linear response theories for interatomic exchange interactions*, J. Phys.: Cond. Matt. **36** 223001 (2024), doi: https://doi.org/10.1088/1361-648X/ad215a.

[32] A. A. Katanin, A. S. Belozerov, A. I. Lichtenstein, M. I. Katsnelson, *Exchange interactions in iron and nickel: DFT+DMFT study in paramagnetic phase*, Phys. Rev. B **107**, 235118 (2023), doi: https://doi.org/10.1103/PhysRevB.107.235118.

[33] P. Giannozzi, et. al., *Quantum ESPRESSO: a modular and open-source software project for quantum simulations of materials*, J. Phys.: Condens. Matter **21**, 395502 (2009), doi: https://doi.org/10.1088/0953-8984/21/39/395502; *Advanced capabilities for materials modelling with Quantum ESPRESSO*, *ibid.* **29**, 465901 (2017), doi: https://doi.org/10.1088/1361-648X/aa8f79; https://www.quantum-espresso.org.

[34] G. Pizzi, et. al., *Wannier90 as a community code: new features and applications*, J. Phys. Cond. Matt. **32**, 165902 (2020), doi: https://doi.org/10.1088/1361-648X/ab51ff; http://www.wannier.org.

[35] P. Porta, M. Marezio, J. P. Remeika, P. D. Dernier, *Chromium dioxide: High pressure synthesis and bond lengths*, Mater. Res. Bull. **7**, 157 (1972), doi: https://doi.org/10.1016/0025-5408(72)90272-3.

[36] A. Hausoel, M. Karolak, E. Sasioglu, A. Lichtenstein, K. Held, A. Katanin, A. Toschi, and G. Sangiovanni, *Local magnetic moments in iron and nickel at ambient and Earth's core conditions*, Nature Communications **8**, 16062 (2017), doi: https://doi.org/10.1038/ncomms16062.

[37] M. T. Czyżyk and G. A. Sawatzky, *Local-density functional and on-site correlations: The electronic structure of La_2CuO_4 and $LaCuO_3$*, Phys. Rev. B **49**, 14211 (1994), doi: https://doi.org/10.1103/PhysRevB.49.14211.

[38] P. Hansmann, N. Parragh, A. Toschi, G. Sangiovanni, and K Held, *Importance of d–p Coulomb interaction for high T_C cuprates and other oxides*, New J. Phys. **16**, 033009 (2014), doi: http://dx.doi.org/10.1088/1367-2630/16/3/033009.

[39] A. A. Katanin, *DFT+DMFT study of exchange interactions in cobalt and their implications for the competition of hcp and fcc phases*, Phys. Rev. B **108**, 235170 (2023), doi: https://doi.org/10.1103/PhysRevB.108.235170.

[40] E. M. Agapov, I. A. Kruglov, A. A. Katanin, *MXene Fe_2C as a promising candidate for the 2D XY ferromagnet*, 2D Mater. **11**, 025001 (2024), doi: https://doi.org/10.1088/2053-1583/ad10bc.

[41] G. Rohringer, H. Hafermann, A. Toschi, A. A. Katanin, A. E. Antipov, M. I. Katsnelson, A. I. Lichtenstein, A. N. Rubtsov, K. Held, *Diagrammatic routes to nonlocal correlations beyond dynamical mean field theory*, Rev. Mod. Phys. **90**, 025003 (2018), doi: https://doi.org/10.1103/RevModPhys.90.025003.

[42] A. A. Katanin, *Generalized dynamical mean-field theory of two-sublattice systems with long-range interactions and its application to study charge and spin correlations in graphene*, Phys. Rev. B **104**, 245142 (2021), doi: https://doi.org/10.1103/PhysRevB.104.245142; *Charge and spin correlations in insulating and incoherent metal states of twisted bilayer graphene*, Phys. Rev. B **106**, 115147 (2022), doi: https://doi.org/10.1103/PhysRevB.106.115147.

[43] A. N. Rubtsov, V. V. Savkin, and A. I. Lichtenstein, *Continuous-time quantum Monte Carlo method for fermions*, Phys. Rev. B **72**, 035122 (2005), doi: https://doi.org/10.1103/PhysRevB.72.035122; P. Werner, A. Comanac, L. de Medici, M. Troyer, and A. J. Millis, *Continuous-Time Solver for Quantum Impurity Models*, Phys. Rev. Lett. **97**, 076405 (2006), doi: https://doi.org/10.1103/PhysRevLett.97.076405.

[44] Li Huang, Y. Wang, Zi Yang Meng, L. Du, P. Werner, and Xi Dai, *iQIST: An open source continuous-time quantum Monte Carlo impurity solver toolkit*, Comp. Phys. Comm. **195**, 140 (2015), doi: http://dx.doi.org/10.1016/j.cpc.2015.04.020; Li Huang, *iQIST v0.7: An open source continuous-time quantum Monte Carlo impurity solver toolkit*, Comp. Phys. Comm. **221**, 423 (2017), doi: http://dx.doi.org/10.1016/j.cpc.2017.08.026.

[45] N. Parragh, G. Sangiovanni, P. Hansmann, S. Hummel, K. Held, and A. Toschi, *Effective crystal field and Fermi surface topology: A comparison of d- and dp-orbital models*, Phys. Rev. B **88**, 195116 (2013), doi: https://doi.org/10.1103/PhysRevB.88.195116.

[46] J. Schmalian, D. Pines, and B. Stojkovic, *Weak Pseudogap Behavior in the Underdoped Cuprate Superconductors*, Phys. Rev. Lett. **80**, 3839 (1998), doi: https://doi.org/10.1103/PhysRevLett.80.3839; *Microscopic theory of weak pseudogap behavior in the underdoped cuprate superconductors: General theory and quasiparticle properties*, Phys. Rev. B **60**, 667 (1999), doi: https://doi.org/10.1103/PhysRevB.60.667.

[47] A. A. Katanin, A. P. Kampf, and V. Yu. Irkhin, *Anomalous self-energy and Fermi surface quasisplitting in the vicinity of a ferromagnetic instability*, Phys. Rev. B **71**, 085105 (2005), doi: https://doi.org/10.1103/PhysRevB.71.085105; A. A. Katanin, *Electronic self-energy and triplet pairing fluctuations in the vicinity of a ferromagnetic instability in two-dimensional systems: Quasistatic approach*, Phys. Rev. B **72**, 035111 (2005), doi: https://doi.org/10.1103/PhysRevB.72.035111; A. A. Katanin and V. Yu. Irkhin, *Spectral functions of two-dimensional systems with coupling of electrons to collective or localized spin degrees of freedom*, Phys. Rev. B **77**, 115129 (2008), doi: https://doi.org/10.1103/PhysRevB.77.115129.

[48] Y. Nomura, S. Sakai, and R. Arita, *Fermi surface expansion above critical temperature in a Hund ferromagnet*, Phys. Rev. Lett. **128**, 206401 (2022), doi: https://doi.org/10.1103/PhysRevLett.128.206401.

[49] S. Sakai, R. Arita, K. Held, and H. Aoki, *Quantum Monte Carlo study for multiorbital systems with preserved spin and orbital rotational symmetries*, Phys. Rev. B **74**, 155102 (2006), doi: https://doi.org/10.1103/PhysRevB.74.155102.

[50] K. Wilson, *The renormalization group: Critical phenomena and the Kondo problem*, Rev. Mod. Phys. **47**, 773 (1975), doi: https://doi.org/10.1103/RevModPhys.47.773.

[51] A. A. Katanin, *Extracting Kondo temperature of strongly-correlated systems from the inverse local magnetic susceptibility*, Nat. Commun. **12**, 1433 (2021), doi: https://doi.org/10.1038/s41467-021-21641-2.

[52] A. Barry, J. M. D. Coey, L. Ranno, and K. Ounadjela, *Evidence for a gap in the excitation spectrum of CrO_2*, J. Appl. Phys. **83**, 7166 (1998), doi: http://dx.doi.org/10.1063/1.367791.

[53] X. W. Li, A. Gupta, and G. Xiao, *Influence of strain on the magnetic properties of epitaxial (100) chromium dioxide (CrO_2) films*, Appl. Phys. Lett. **75**, 713 (1999), doi: http://dx.doi.org/10.1063/1.124491.

[54] P. Lubitz, M. Rubinstein, M. S. Osofsky, B. E. Nadgorny, R. J. Soulen, K. M. Bussmann, and A. Gupta, *Ferromagnetic resonance observation of exchange and relaxation effects in CrO_2*, Journ. Appl. Phys. **89**, 6695 (2001), doi: http://dx.doi.org/10.1063/1.1362636.

[55] J. Rusz, I. Turek, and M. Diviš, *Random-phase approximation for critical temperatures of collinear magnets with multiple sublattices: GdX compounds (X=Mg,Rh,Ni,Pd)* Phys. Rev. B **71**, 174408 (2005), doi: https://doi.org/10.1103/PhysRevB.71.174408.

[56] A. Toschi, G. Rohringer, A. A. Katanin, and K. Held, *Ab initio calculations with the dynamical vertex approximation*, Annalen der Physik, **523**, 698 (2011), doi: https://doi.org/10.1002/andp.201100036.

[57] E. A. Stepanov, E. G. C. P. van Loon, A. A. Katanin, A. I. Lichtenstein, M. I. Katsnelson, and A. N. Rubtsov, *Self-consistent dual boson approach to single-particle and collective excitations in correlated systems*, Phys. Rev. B **93**, 045107 (2016), doi: https://doi.org/10.1103/PhysRevB.93.045107.

[58] M. Vandelli, J. Kaufmann, M. El-Nabulsi, V. Harkov, A. I. Lichtenstein, and E. A. Stepanov, *Multi-band D-TRILEX approach to materials with strong electronic correlations*, SciPost Phys. **13**, 036 (2022), doi: https://doi.org/10.21468/SciPostPhys.13.2.036.

[59] J. A. Hertz and D. M. Edwards, *Electron-magnon interactions in itinerant ferromagnetism. I. Formal theory*, J. Phys. F **3**, 2174 (1973), doi: https://doi.org/10.1088/0305-4608/3/12/018.

[60] K. Momma and F. Izumi, *VESTA 3 for three-dimensional visualization of crystal, volumetric and morphology data*, J. Appl. Crystallogr. **44**, 1272 (2011), doi: https://doi.org/10.1107/S0021889811038970.

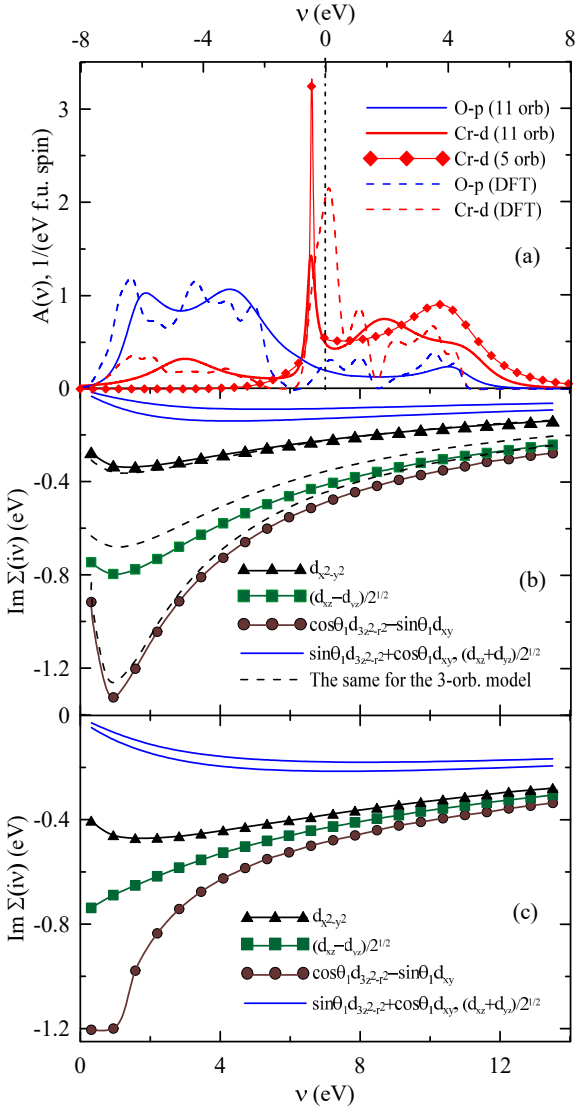

Figure 2: The DFT (dashed lines) and DFT+DMFT (solid lines) partial densities of states at the real frequencies (a) and the imaginary part of the self-energy at the imaginary frequency axis for states of different symmetry in five-orbital (solid lines), three-orbital (dashed lines) (b) and 11-orbital (c) model at $\beta = 10$ eV^{-1} in the DFT+DMFT approach with on-site Coulomb repulsion.

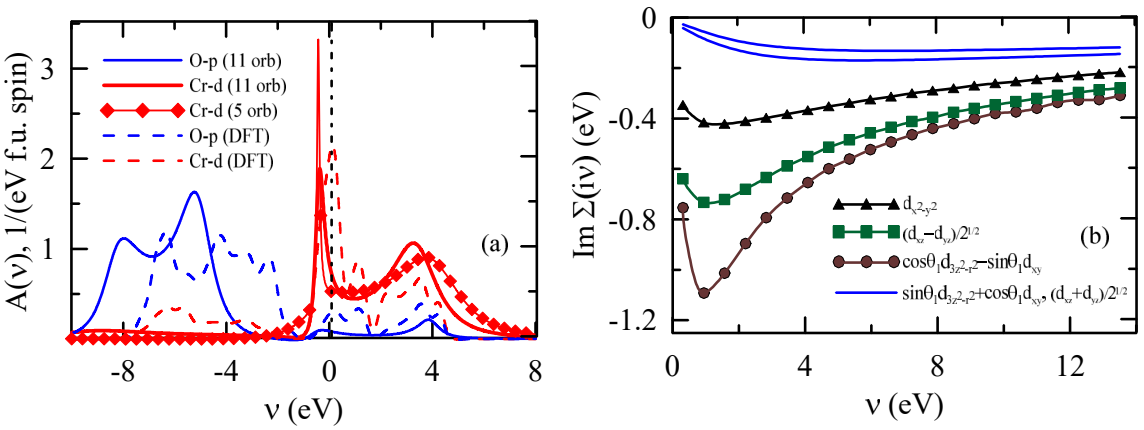

Figure 3: Spectral functions (a) and electronic self-energies (b) in the 11-orbital model with account of U_{pp} and non-local U_{dp} interactions

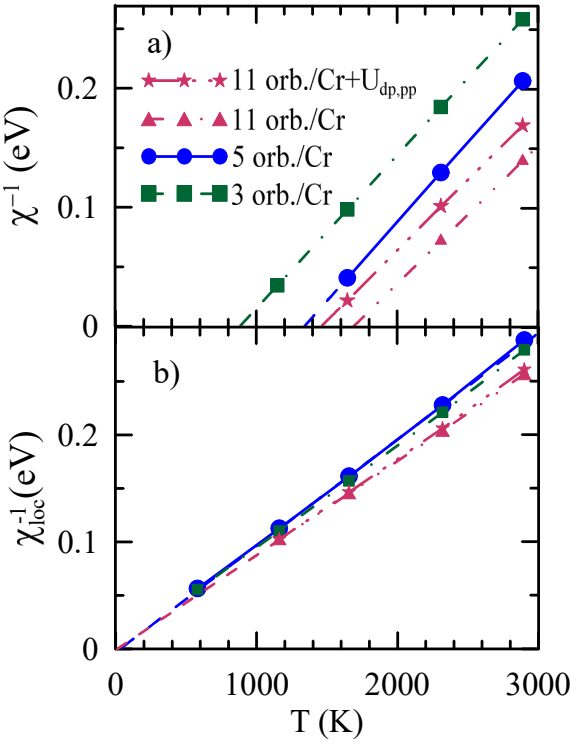

Figure 4: Temperature dependence of the inverse longitudinal uniform (a) and local (b) susceptibilities of CrO_2 within the DFT+DMFT approach. Solid blue lines correspond to the five-orbital model per Cr site, dot-dashed green lines correspond to the three-orbital model, red dot-dot-dashed (dot-dot-dot-dashed) lines to the 11 orbital model per Cr site, including oxygen states without (with) additional U_{dp} and U_{pp} interactions.

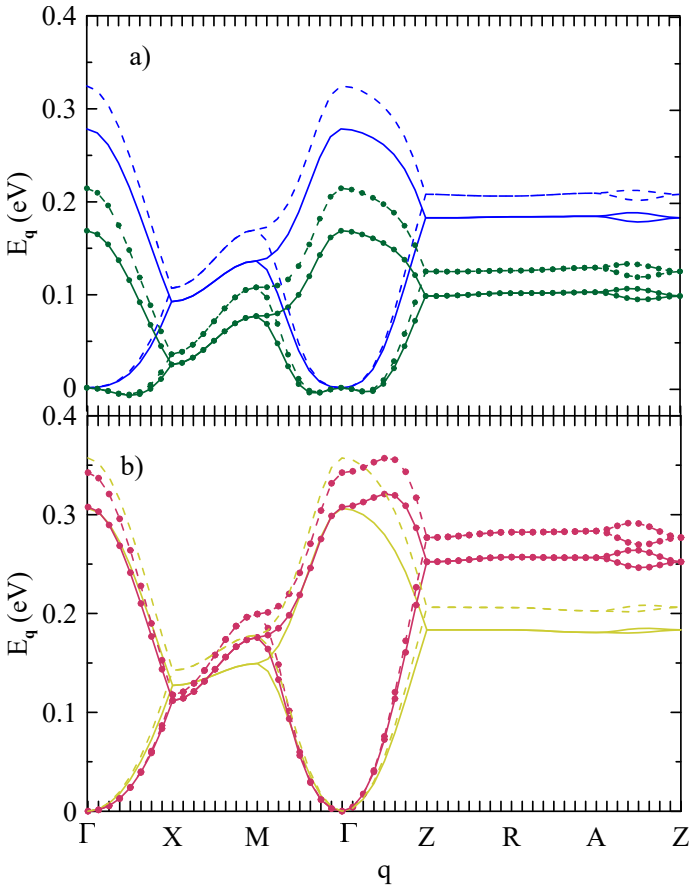

Figure 5: Magnon dispersion at $\beta = 7$ eV^{-1} (solid lines) and $\beta = 10$ eV^{-1} (dashed lines) (a) in the models with three (green lines with symbols) and five orbitals (blue lines) per Cr site and (b) in the models with 11 orbitals per Cr site which includes oxygen states, with (dark yellow lines) or without (red lines with symbols) additional U_{dp} and U_{pp} interactions.

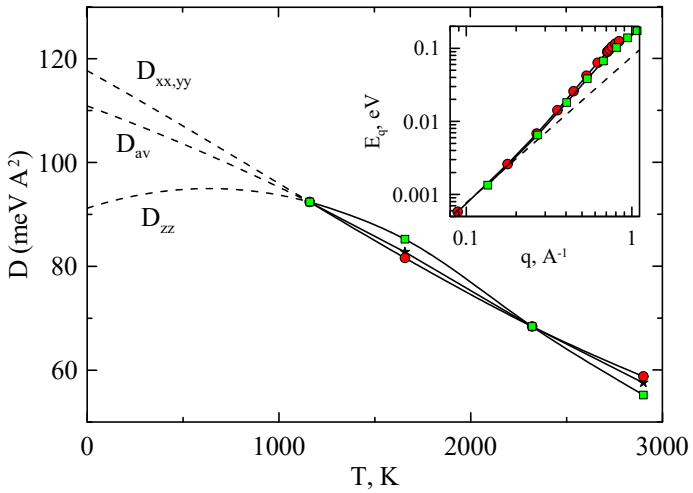

Figure 6: Temperature dependencies of the obtained spin-wave stiffnesses in the x, y (red circles) and z (green squares) directions, together with the average spin-wave stiffness $D_{\text{av}} = (D_{xx}^2 D_{zz})^{1/3}$ (black stars) in the five-orbital model. Dashed lines show the result of extrapolation. The inset shows momentum dependencies of magnon energies at $\beta = 10$ eV^{-1} in the respective directions in logarithmic scale, dashed line corresponds to quadratic fit.

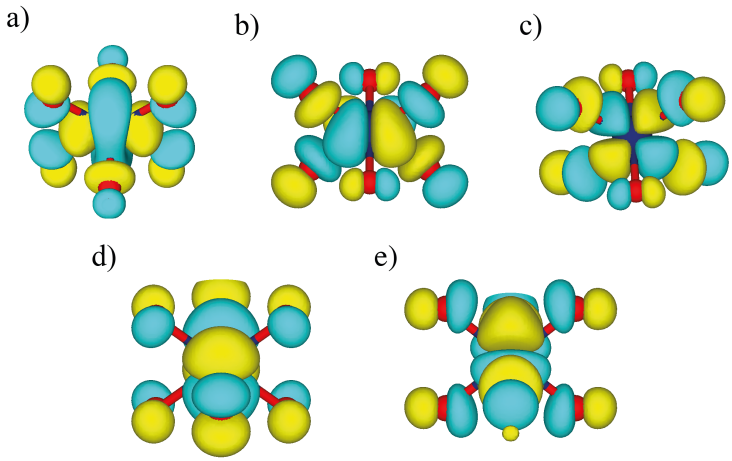

Figure 7: Visualization of Wannier orbitals in 5-orbital model (per Cr site), including only d states. Blue circles in the center (partly hidden by Wannier orbitals) correspond to chromium atom, red lines and circles show the bonds and oxygen atoms.

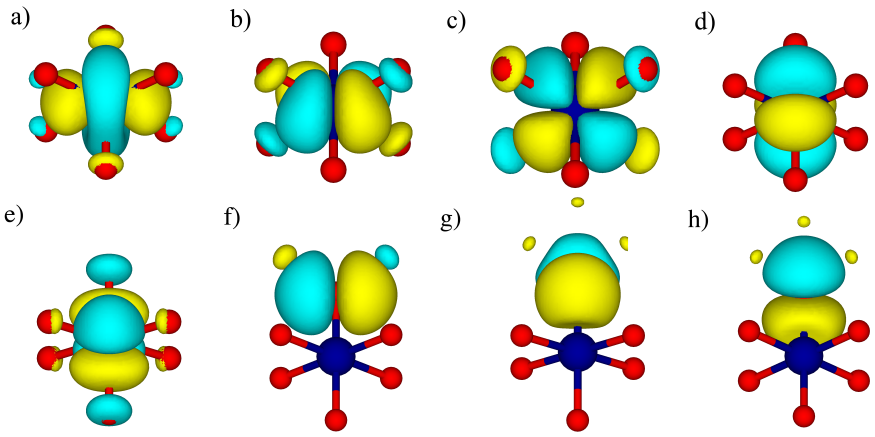

Figure 8: Visulaization of Wannier orbitals in 11-orbital model (per Cr site) at chromium (a-e) and one of the oxygen (f-h) sites. The notations are the same as in Fig. 7.